IEEE Photonics Journal
An IEEE Photonics Society Publication

Open Access

Effect of Temperature on Supercontinuum Generation in CS_2-Core Optical Fiber

Volume 10, Number 5, September 2018

Chao Wang
Guoying Feng
Wei Li
Jinliang Men
Xiaoxu Chen
Chao Yang
Shouhuan Zhou

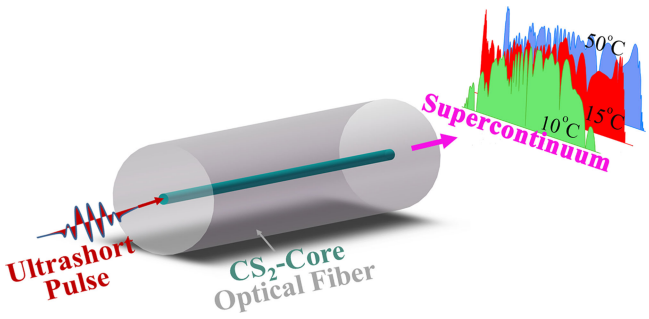

DOI: 10.1109/JPHOT.2018.2865576
1943-0655

IEEE photonics SOCIETY

IEEE

Effect of Temperature on Supercontinuum Generation in CS_2-Core Optical Fiber

Chao Wang,[1] Guoying Feng,[1,2] Wei Li,[1] Jinliang Men,[1] Xiaoxu Chen,[1] Chao Yang,[1] and Shouhuan Zhou[1,2]

[1]Institute of Laser & Micro/Nano Engineering, College of Electronics & Information Engineering, Sichuan University, Chengdu 610064, China
[2]North China Research Institute of Electro-optics, Beijing 100015, China

DOI:10.1109/JPHOT.2018.2865576

Manuscript received May 18, 2018; revised August 7, 2018; accepted August 10, 2018. Date of current version September 13, 2018. This work was supported by the National Natural Science Foundation of China for Youth (NSFC, no. 11704268), the Joint Funds of the National Nature Science Foundation and the China Academy of Engineering Physics Foundation (NSAF, no. U1430126) and Open Research Fund of Key Laboratory of High Energy Laser Science (CAEP, no. 2013HEL05). Corresponding author: Guoying Feng (e-mail: guoing_feng@scu.edu.cn; 1419901623@qq.com).

Abstract: We investigate the effect of temperature on the supercontinuum generation of CS_2 single-hole liquid core optical fiber (LCOF). By solving the generalized nonlinear Schrödinger equation, the effect of the temperature on spectral broadening, coherence, soliton effects, and modulation instability was analyzed. The results turn out that the supercontinuum generation by pumping the LCOP with 1.95-μm laser is robust over a broad temperature range (15–45 °C). The optimal temperature to generate the broadest spectrum of SC via LCOF is 15 °C, which is independent on the pump power. The coherence of the generated SC is independent on the temperature at low pump power (such as $P_0 = 4$ kW), while at a high pump power (such as $P_0 = 40$ kW) the coherence of the long wave (around 2600 nm) tends to be deteriorated at low temperature (e.g., 10 °C). The underlying reason for such phenomenon has been discussed as well.

Index Terms: Liquid core optical fiber, soliton fission, modulation instability, supercontinuum generation.

1. Introduction

Supercontinuum generation (SCG) is the broadening of the pulse spectrum by the propagation of sufficiently intense incident pulses through non-linear media. At present, SCG, especially in infrared-region, is of great importance [1], since it can be used for nonlinear spectroscopy (e.g., pump-probe spectroscopy [2], coherent Raman spectroscopy [3], near-field optical microscopy identification of molecular species [4]), in optical coherence tomography (OCT) [5], photoacoustic imaging [6], coherent optical communication [7], optical frequency metrology and other fields. Studies have shown that anomalous dispersion pump can provide a wider spectrum than the normal dispersion region [8], [9]. The mechanism of SCG has been studied extensively, and it is considered a combination of self-phase modulation (SPM), soliton fission [10], cross-phase modulation (XPM) [11], [12], stimulated Raman scattering (SRS) [13], four-wave mixing (FWM) [14], and properties of the fiber [15]. Among these nonlinear phenomena, SPM dominates during the first few centimeters of propagation, then the soliton fission accompanied by the radiation emission and reflection of the dispersive waves from emerging solitons lead to further spectral broadening. Soliton was proposed

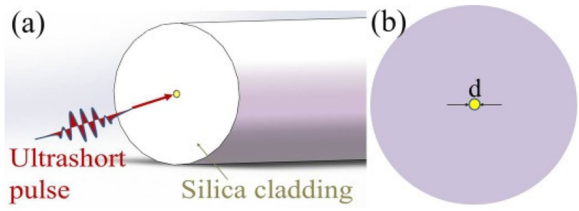

Fig. 1. Fiber Design. (a) Schematics of SCG via liquid core optical fiber, (b) cross-sectional of LCOF with diameter d = 4.0 μm.

by Hasegawa and Tapert [16], which originated from the balance of anomalous dispersion and self-phase modulation. The next stage is the Raman shifted solitons on the long-wavelength edge of the supercontinuum enter into the regime of the cascaded interaction with dispersive radiation [17]. This quickly leads to the formation of the bound soliton-radiation states responsible for continuous spectral divergence of the supercontinuum edges [18]. The necessary condition for this to occur is the near matching of the group velocities across the zero GVD point [19]. Husakou and Herrmann proposed a complete theory of SCG by taking advantage of soliton related effects in 2001 [10], and demonstrated that the spectral broadening through fission of higher-order soliton into redshifted fundamental solitons (induced by Raman scattering) and blueshifted nonsolitonic radiation and confirmed by experiments.

Ultra-broadband SCG is achieved by modulation instability (MI) [20]–[25] besides soliton fission [19], [26], [27] in the anomalous dispersion region. MI-induced ultra-broadband spectroscopy was first proposed by Hasegawa and Brinkman in 1980 [22]. The MI, at the expense of the absorption of two pump photons, can be explained by the four-wave mixing (FWM) process of phase matching through nonlinear and dispersion effects, leading to exponential growth of the Stokes and anti-Stokes sidebands [26]. In addition to noise induced MI, it is also possible to initiate the process by feeding with a countersignal at a frequency separation from the pump lying within the gain window [21].The MI turns out to dominate higher-order effects such as third-and fourth-order dispersion, self-steepening and stimulated Raman scattering [20].

Most research on soliton-based SCG emerge in novel and hybrid material waveguide, such as soft-glass systems (e.g., chalcogenides, tellurides, filuorides), making use of their significantly higher nonlinearity and wider transmission windows, particularly towards mid-infrared wavelength [28]. Likewise, highly nonlinear liquid-filled (CS_2) optical fibers have properties comparable to those of soft-glass. Several works studied the SC generation in the anomalous dispersion regime of hollow-core fibers filled with CS_2 [27], [29]. However, the diameter of the filled center hole is less than 3 μm in the above articles, which posts some difficulties to the optical path coupling in practical experiments. A recent work studied the SC broadening of CS_2 single-hole liquid core in the anomalous dispersion region at room temperature (20 °C) [30]. However the effects of temperature variation on SCG have not been taken into consideration.

In this paper, the supercontinuum generation (SCG) by a liquid core optical fiber (LCOF) is numerically studied. The optimal condition for SCG, including but not limited to, operating temperature, is discussed. The effect of temperature and pump peak powers on the properties of supercontinuum is researched. This study will potentially contribute to the optimization of the SCG using CS_2 single-hole liquid core optical fiber.

2. Design of LCOF and Theoretical Model

2.1 Fiber Design and Characterization for Supercontinuum Generation

We first design a reasonable liquid core optical fiber (LCOF) for supercontinuum generation (SCG). Fiber structure is shown in Fig. 1. The zero-dispersion wavelength (ZDW) of the LCOF lies in the IR window, for which the pump wavelength $\lambda = 1.95$ μm is selected. The refractive index of CS_2 is

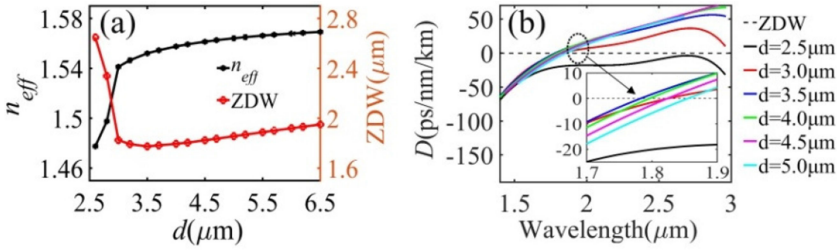

Fig. 2. Characteristics of LCOF; (a) GVD map: the spectral position of the ZDW (abnormal dispersion) varying with different core diameters at 20 °C. (b) GVD of the fundamental mode (HE11) of the LCOF. The inset shows the details of the ZDW. Fig. 2 was calculated by using Eq. (1)–(4).

calculated by the following Sellmeier (20 °C) equation [30]:

$$n_{20}^2(\lambda) - 1 = \frac{1.499426\lambda^2}{\lambda^2 - (0.178763)} + \frac{0.089531\lambda^2}{\lambda^2 - (6.591946)}, \tag{1}$$

λ is the wavelength (μm) in vacuum. The temperature-dependent refractive index n(λ, T) is governed by the formula [31]:

$$n(\lambda, T) = n_{20}(\lambda) + \Delta T \left(\frac{dn}{dT}\right), \tag{2}$$

where T represents the desired temperature, and ΔT is the difference between T and 20 °C, dn/dT indicates gives the rate of variation of refractive indices with temperature, and dn/dT $= -7.91 \times 10^{-4}$ K^{-1} for CS_2 [31], [32], since the silica has temperature-dependent refractive index [24]. In order to calculate the $n_{eff}(\lambda)$ and the effective area A_{eff} [33] of the LCOF, we use the full-vector finite element method (FEM) [33]–[35] and assume the anisotropic perfectly matched layers (PML). The total dispersion of the LCOF structure can be well approximated using the following relation

$$D(\lambda) = D_w(\lambda) + D_m(\lambda), \tag{3}$$

where D(λ) is the total dispersion of the fiber, $D_w(\lambda)$ is the waveguide dispersion, and $D_m(\lambda)$ is the material dispersion which can be obtained using the Sellmeier's equation. And the exact definition of the total chromatic dispersion as:

$$D(\lambda) = -\frac{\lambda}{c}\frac{d^2 \mathrm{Re}[n_{eff}(\lambda)]}{d\lambda^2} = -\frac{2\pi c}{\lambda^2}\beta_2, \tag{4}$$

where c, β_2 and $n_{eff}(\lambda)$ are the velocity in free space, the second-order dispersion, and the LCOFs effective index of the fundamental mode respectively, the material dispersion based on Sellmeier's equation has been taken into account explicitly in the effective index of the LCOF [36]. If the input pulse center wavelength approaches the zero-dispersion wavelength (ZDW), $\beta_2 = 0$. Applying the FEM, we determined the chromatic dispersion referred as the group velocity dispersion (GVD) as a function of the wavelength of the fundamental mode at different temperature shown in Fig. 2(b). It is clearly that the ZDW move towards the pump wavelength as the temperature increases. Fig. 2(b) also implies the blue-shift of ZDW could be done by reducing the core-diameter of LCOF. However, the amount of blue-shift is limited before the core diameter of LCOF becomes too small to fabricate. For practical reason, we limit the diameter of LOCF between 3.0 μm to 6.5 μm, which provide a broad zero-dispersion wavelength (ZDW) range between 1.825 μm and 1.950 μm for SC generation.

Contrast to solft-glass fibers where subwavelength core diameters are required [38], the core diameter of LOCF can be between 3.0 μm and 6.50 μm, and the zero-dispersion wavelength (ZDW) (Fig. 2) point is between 1.825 μm and 1.950 μm. These parameters meet the working conditions in anomalous dispersion region, and in turn make the spectrum broadening effectively. The normalized frequency of step index guided fiber, defined with V-parameters, can be

described with

$$V = \frac{\pi d}{\lambda} \cdot \sqrt{n_{core}^2 - n_{clad}^2}, \tag{5}$$

where d is the diameter of the fiber core, n_{core} and n_{clad} are the core and cladding index respectively. When choosing the diameter d = 4.0 μm for LOCF, Eq. (5) yields V = 4.24 larger than characteristic value of V = 2.405 for fundamental mode working state [39]. Despite high-order modes have contributions to supercontinuum generation (SCG) [40], [41], the fundamental mode still dominates in SCG in LOCF with the length of 0.1 m. Therefore, in this paper, we consider only the contribution of the fundamental mode in LCOF.

2.2 Nonlinear Pulse Propagation

To describe nonlinear pulse propagation in the CS_2 liquid filled LCOF, the generalized nonlinear Schrodinger equation (GNLSE) [42] is solved by using the improved Runge-Kutta algorithm [43]:

$$\frac{\partial A}{\partial z} = -\frac{\alpha}{2} - \left(\sum_{k\geq 2} \beta_n \frac{i^{n-1}}{n!} \frac{\partial^n}{\partial \tau^n}\right) A + i\gamma \frac{1}{\omega_0}\left(1 + \frac{\partial}{\partial \tau}\right) \times \left[(1 - f_R)A|A|^2 + f_R A \int_0^\infty h_R(t')\left|A(z, \tau - t')\right|^2 dt'\right], \tag{6}$$

where A(z, τ) is the envelope of the electric field, α is the propagation loss, β_n is the n-th order dispersion coefficient, f_R and $h_R(t)$ are Raman contributions and CS_2 Raman response function [42], here z is the propagation length and τ ($\tau = (t - \beta_1 z)$, β_1^{-1} is the group velocity) is the time measured in the reference frame moving with the group velocity at the pump frequency [19]. We use a hyperbolic secant pulse with large duration $T_0 = 352$ fs determined with FWHM. The first term on the right-hand side of Eq. (6) is the loss term, the second term represents the dispersion terms, and the third term includes self-phase modulation, cross-phase modulation, quaternion mixing, stimulated Raman scattering and self-steepness.

The optical pulse response function is:

$$R(t) = (1 - f_R)\delta(t) + f_R \cdot h_R(t), \tag{7}$$

the fractional f_R contribution of Raman response is as high as 0.89 and the normalized Raman response function $h_R(t)$ can be written as follows [46]:

$$h_R(t) = 0.5048 \cdot \exp\left(-\frac{t}{\tau_{diff}}\right)\left[1 - \exp\left(-\frac{t}{\tau_{rise}}\right)\right] + 0.8314 \cdot \exp\left(-\frac{t}{\tau_{\text{int}}}\right)\left[1 - \exp\left(-\frac{t}{\tau_{rise}}\right)\right] + 1.633 \cdot \exp\left(-\frac{\alpha^2 t^2}{2}\right) \sin(\omega_0 t), \tag{8}$$

where $\tau_{\text{diff}} = 1.68$ ps, $\tau_{\text{rise}} = 0.14$ ps, $\tau_{\text{int}} = 0.4$ ps, $\alpha = 5.4$/ps, $\omega_0 = 6.72$/ps.

Coherence is an essential parameter of supercontinuum generation (SCG). This is because from a practical point of view, the supercontinuum (SC) light source is required to be highly coherent if it is utilized for applications such as optical metrology. For this reason, the coherence properties of SC have gained significant interest, so we calculate the first-order coherence of the spectrum by introducing Gaussian white noise [44]:

$$\left|g_{mn}^{(1)}(\lambda)\right| = \left|\frac{\left\langle E_m^*(\lambda)E_n(\lambda)\right\rangle}{\sqrt{\left\langle\left|E_m(\lambda)\right|^2\right\rangle\left\langle\left|E_n(\lambda)\right|\right\rangle^2}}\right|, \tag{9}$$

where E(λ) denotes the electric field at the wavelength λ, m and n denote the indices of the individual spectra ($m \neq n$), and the angular brackets refer to an ensemble average. In this paper, 50 individual spectrum are used to calculate the first order coherence under identical input conditions

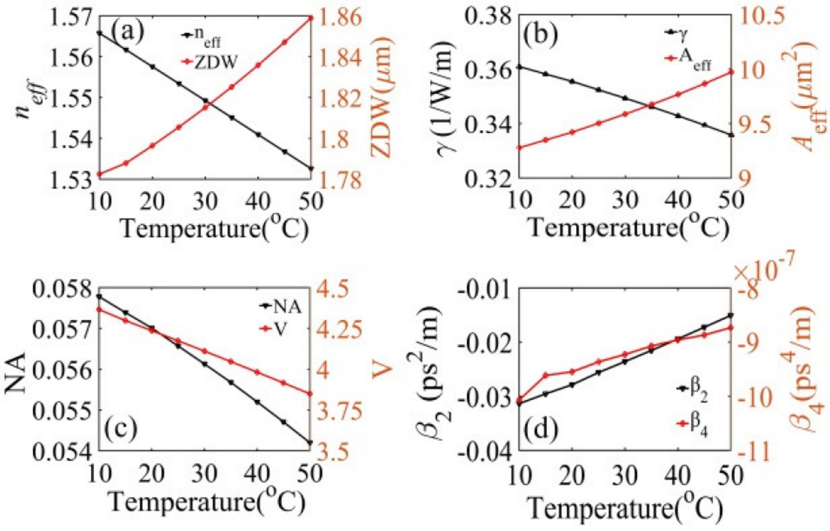

Fig. 3. Influence of temperature on fiber parameters. (a) Variation of n_{eff} and ZDW, (b) nonlinear parameter γ and effective area A_{eff} and (c) and NA and V parameter, (d) β_2 and β_4 as a function of temperature of LCOF, the core diameter d = 4.0 μm. Fig. 3(a) was calculated by using Eq. (1)–(4), Fig. 3(b), (c), (d) were calculated by using Ref. [37].

with random Gaussian white noise. The values of $|g_{mn}^{(1)}(\lambda)|$ at each wavelength are closer to 1, the better the coherence of SC.

3. Numerical Results and Discussion

The following parameters were used throughout this paper: a) the LCOF core diameter d = 4.0 μm; b) the hyperbolic secant pulse with large duration T_0 = 352 fs; c) the fiber length L = 0.1 m; d) the pump center wavelength is λ = 1.95 μm; e) nonlinear refractive index $n_2 = 1.04 \times 10^{-18}$ m^2W^{-1}; f) in the effect of temperature on modulation instability (MI) and soliton fission for supercontinuum generation, our pump power are P_0 = 4 kW, 8 kW, 16 kW, 40 kW, respectively.

3.1 Influence of Temperature on Fiber Parameters

SCG results from the interaction of high-order nonlinear terms such as self-phase modulation with fiber dispersion. Therefore, the variation of temperature will lead to the changes of the parameters of LCOF, e.g., the effective index n_{eff}, the dispersion coefficients β_n, mode field effective area A_{eff}, and the spectral bandwidth of supercontinuum, and resultantly influence SCG.

It can be seen from Fig. 3 that the dispersion coefficient β_n (ps^n/m), and the nonlinear coefficient γ, the effective area A_{eff}, the numerical aperture (NA) and the V-parameter of the LCOF are temperature-dependent. The zero-dispersion wavelength (ZDW) (Fig. 3(a) increases from 1.782 μm to 1.859 μm while the nonlinear coefficients γ (Fig. 3(b)) decreases from 0.36093 $W^{-1}m^{-1}$ to 0.33580 $W^{-1}m^{-1}$ when the temperature of the LCOF increases from 10 °C to 50 °C. The results show that with increasing temperature the ZDW has undergone a redshift, getting closer to the pump wavelength, but the nonlinear coefficient has an opposite trend. Furthermore, the variation on both γ and ZDW's will induce severe changes in the pulse-width. Moreover, Fig. 3(b) and Fig. 3(c) tell that the change on effective area A_{eff} and NA is trivial, and they do not have noticeable effect on the initial optical coupling. Notably, the second-order dispersion coefficient β_2 (Fig. 3(d)) increase from $-3.13607722 \times 10^{-2}$ ps^2/m to $-1.50819699 \times 10^{-2}$ ps^2/m, while the fourth-order nonlinear coefficient β_4 (Fig. 3(d)) decreases from $-1.00690456 \times 10^{-6}$ ps^4/m to $-8.73322714 \times 10^{-7}$ ps^4/m when temperature increases from 10 °C to 50 °C.

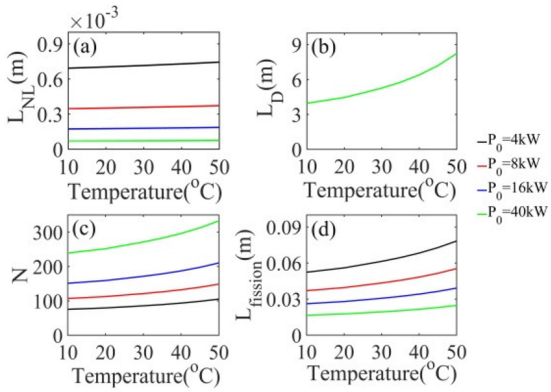

Fig. 4. Influence of temperature on the parameter of supercontinuum generation (SCG); Variation of (a) nonlinear length L_{NL} (b) dispersion length L_D (c) soliton numbers N and (d) soliton splitting length $L_{fission}$ as a function of temperature for different pump power. Fig. 4 was obtained by using Ref. [37].

3.2 The Effect of Temperature on Modulation Instability and Soliton Fission for SCG

In order to simulate SCG, the soliton orders, the length of soliton splitting, and the gain of MI [45] should be considered.

The high-order soliton splits into a large number of fundamental solitons, and the fundamental solitons are amplified through modulation instability (MI) gain, resulting in further broadening of the pulse. The MI gain of a LCOF can be expressed as [22], [23]:

$$G(\Omega, T) = 4\sqrt{\gamma(T)^2 P_0^2 - \left[\gamma(T)P_0 + \beta_2(T)\frac{\Omega^2}{2} + \beta_4(T)\frac{\Omega^2}{24}\right]^2}, \tag{10}$$

Eq. (10) reveals the effect of temperature on the gain bandwidth is due to a change in the dispersion coefficient as a function of temperature.

The simulation results were given in Fig. 4. Fig. 4(a) shows that as the temperature increases from 10 °C to 50 °C with an interval of 5 °C, the nonlinear length L_{NL} increases with the temperature in a linear manner at the pump peak power $P_0 = 4$ kW and 8 kW and becomes constant at high pump power (such as $P_0 = 16$ kW, 40 kW) (While, the dispersion length L_D (Fig. 4(b)) increases exponentially with temperature increasing from 10 °C to 50 °C, and the length claims for phase matching conditions to generate new photons also varies. The soliton order N (Fig. 4(c)) and soliton fission length $L_{fission}$ (Fig. 4(d)) increase with the temperature in the temperature range from 10 °C to 50 °C.

Modulation instability (MI) is a special four-wave mixing (FWM) process, which is dominant for short propagation lengths forming two distinct side peaks in IR and blue, the entire process continues in a chain reaction until the spectrum is greatly broadened. From Eq. (10), it is obtained that the phase matching condition for the process of MI is influenced by β_2, β_4 which is a function of the temperature of the LOCF [23]. In order to study the effect of temperature on modulation instability (MI), we plot the Stokes lines in the mid-IR region (Fig. 5) of different temperature at pump power $P_0 = 4$ kW, 40 kW (a, d). It is obvious that the MI gain is affected not only by the pump power but also by the temperature. The peaks of the MI gain show a small amount of decreasing trend at the same peak pump power and the corresponding frequency shift is increasing. The variation of bandwidth of MI spectrum $\triangle\lambda$ varies with different pump powers, such as $\triangle\lambda = 26$ nm, 30 nm, 34 nm, 40 nm at pump power $P_0 = 4$ kW, and $\triangle\lambda = 34$ nm, 26 nm, 30 nm, 28 nm at pump power $P_0 = 40$ kW, as the temperature increases from 10 °C to 50 °C with an interval of 10 °C. However, the higher the pump power, the less obvious their changes are. It meant that the influence of the temperature on the supercontinua generation is different at different pump power. Generally, lower temperature yields higher MI.

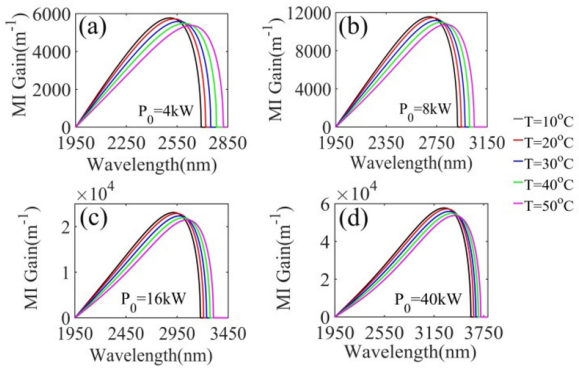

Fig. 5. Variation of MI gain and frequency shift as a function of temperatures. (a–d) MI Gain at different pump power, $P_0 = 4$ kW, 8 kW, 16 kW, 40 kW respectively. Fig. 5 was calculated by using Eq. (10).

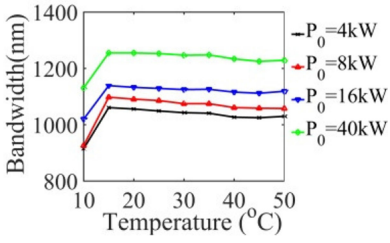

Fig. 6. Variation of (−30 dB) bandwidth as a function of temperature for different pump power. Fig. 6 was calculated by using Eq. (6)–(8).

TABLE 1

Pulse Break-Up Distance, Spectral Position, and Bandwidth for Different Combination of Pump Power $P_0 = 4$ kW

Temp (°C)	$L_{fission}$ (cm)	Lower edge (nm)	Higher edge (nm)	Bandwidth (nm)
10	5.24	1636	2551	915
15	5.42	1569	2630	1061
50	7.83	1581	2611	1030

PUMP POWER P_0=40 kW.

Temp (°C)	$L_{fission}$ (cm)	Lower edge (nm)	Higher dge (nm)	Bandwidth (nm)
10	1.66	1622	2753	1131
15	1.71	1529	2784	1255
50	2.48	1539	2768	1229

3.3 Influence of Temperature on Spectrum Broadening

The effect of temperature on the amount of spectral broadening is shown in Fig. 6. It is found that the bandwidth firstly increases as temperature increases and then decreases after reaching a maximum value at a temperature of about 15 °C even for different pump power. It implies that the optimal temperature to obtain the broadest SC is 15 °C, which is independent with the pump power.

The variation of spectral bandwidth with respect to temperature is shown in Table 1 as well, the bandwidth reaches a maximum value 1061 nm and 1255 nm at pump power $P_0 = 4$ kW, 40 kW

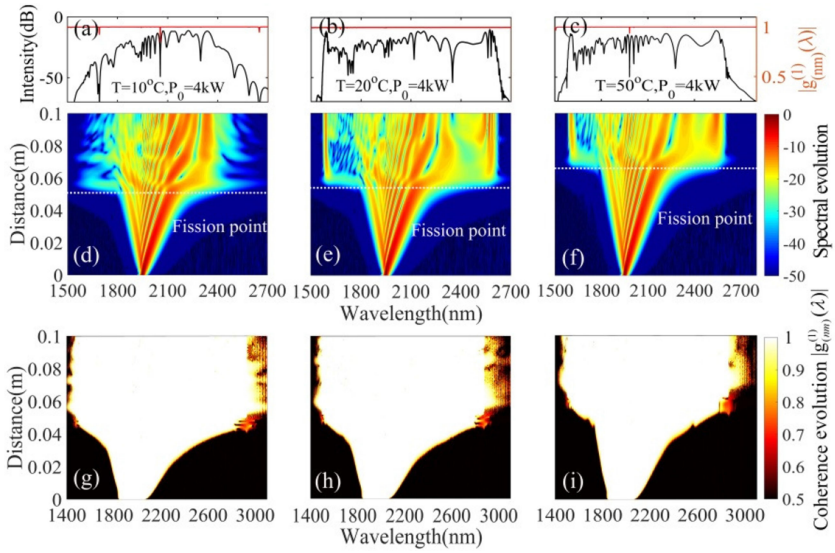

Fig. 7. The output spectra and the first-order coherence (a–c), spectral evolution (d–f) and coherence evolution (g–i) of the propagating pulse with a pump power of 4 kW for temperatures 10 °C, 20 °C, T = 50 °C. The output spectra and spectral evolution (Fig. 6(a–f)) were calculated by using Eq. (6)–(8), and the first-order coherence (Fig. 6(a–i)) was obtained by using Eq. (9).

respectively. This is due to the fact that dispersion and non-linear strong interactions result in maximum spectral broadening, then show a weak downward trend, this is mainly due to the fact that the ZDW move towards the pump wavelength (Fig. 3(a)) but the nonlinear parameter decreases as temperature increases (Fig. 3(b)). The reduction of the spectrum bandwidth is about 30 nm from 15 °C to 50 °C while the increment of the spectrum bandwidth is in proximity of 150 nm from 10 °C to 15 °C. Considering the operating temperature in reference [32] and CS_2 has a boiling point of 46.3 °C, so the working temperature should not be higher than 45 °C. Thus the actual temperature should be kept in 15 °C–45 °C.

3.4 Influence of Temperature on Coherence

Here we shift our attention toward the evolution of the pump pulse with perturbation along the propagation distance. The external perturbation, such as a hyperbolic secant pulse with small amplitude and phase perturbation will bring about the variation of pulse broadening and the first-order coherence. The coherence was proved depending strongly on the input pulse's duration and wavelength, and optimal conditions for coherent supercontinuum generation [44].

We plot the generated supercontinuum (SC) spectra and its first-order coherence (Fig. 7(a–c)) at $P_0 = 4$ kW. It is found that when the temperature increase from 10 °C to 50 °C the soliton frequency is extended from its central wavelength 1950 nm to both sides, providing a broader spectrum width of SCG. Meanwhile, the first-order coherence of the generated SC is around 1, revealing that the first-order coherence is independent of temperatures at a low pump power $P_0 = 4$ kW.

Furthermore, the spectral and temporal evolution of the pump pulses propagated along the LCOF were also investigated, and the results are plotted in Fig. 7(d–f). It was found that $L_{fission}$ becomes longer when the temperature increases, which matches the calculated value well in Fig. 4(d). Moreover, the evolution of the first-order coherence of the generated supercontinuum (SC) is shown in Fig. 7(g–i). It is found that the coherence of the generated SC increases with the propagation depth in the fiber, while the long-wave region of the generated SC has poorer coherence than other spectral components. This is mainly because as the temperature increases, the require working length of the optical fiber becomes bigger. When the pulse continues to transmit, the soliton occurs Raman self-frequency shift, broadening the spectrum to longer waves.

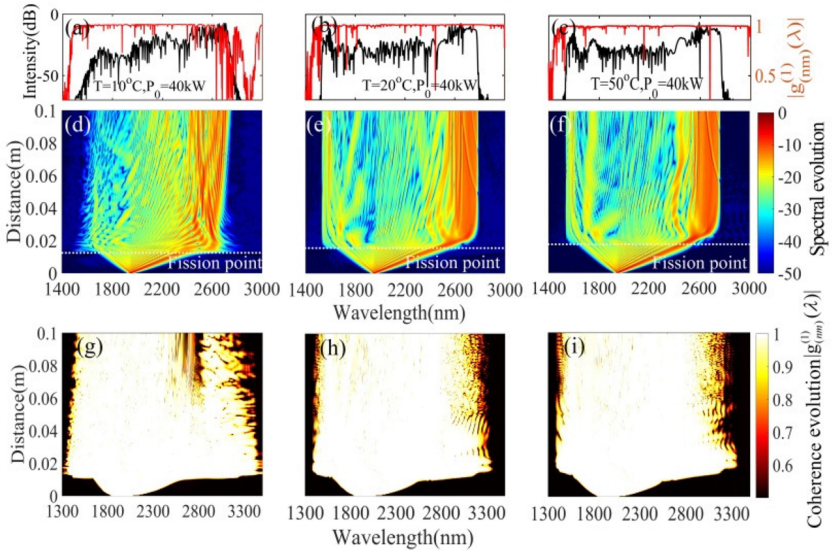

Fig. 8. The output spectra and the first-order coherence (a–c), spectral evolution (d–f) and coherence evolution (g-i) of the propagating pulse with a pump power of 40 kW for temperatures 10 °C, 20 °C, T = 50 °C. The output spectra and spectral evolution (Fig. 7(a–f)) were calculated by using Eq. (6)–(8), and the first-order coherence (Fig. 7(a–i)) was obtained by using Eq. (9).

In order to investigate the effect of different peak pump power on SCG, a similar process was simulated for the case with high pump power $P_0 = 40$ kW, compared with the case at low pump power $P_0 = 4$ kW. The first-order coherence of the SCG at $P_0 = 40$ kW undergoes a large change at different temperatures (Fig. 8(a–c), while that at $P_0 = 4$ kW keep constant with the temperature. Furthermore, the coherence in the entire spectral range is deteriorated (Fig. 8(g–i)). The mainly reason is that MI has a larger gain and acts on the entire spectrum, which leads to the coherence of the output spectrum to deteriorate.

The spectral evolution of the generated SC (Fig. 8(d–f)) tells the higher the peak pulse power, the wider the spectrum will be generated in a shorter distance, but the coherence of the resulting SC will be significantly deteriorated. This is due to more soliton fission occurs in a short distance, the soliton fission length increase with the temperature (see Fig. 4). Raman self-frequency shifting occurs for each soliton, and multiple soliton frequency shifts will cover the entire long-wavelength spectrum when the pump power is $P_0 = 40$ kW. Peak power increases with the MI-gain increase; the Raman auto-frequency shift amplifies the noise at the long wavelength of the MI amplification to produce a long-wave spectrum of the SC. At the same time, the dispersive wave generated by multiple soliton radiations will cover the entire short wave range so that the MI will affect the entire SC generated under the condition of high pump power.

4. Conclusion

Based on the full vector finite element method, the performance parameters of the fiber at different temperatures were simulated and analyzed. Based on this, the effect of the temperature on spectral broadening, coherence, soliton effects and modulation instability was analyzed. The simulation analysis results show: the ZDW of the fiber is red-shifted and gradually close to the pump wavelength, but the nonlinear coefficient of the fiber is reduced as temperature increases.

It was found that when the temperature increased from 10 °C to 50 °C the soliton frequency was extended from its central wavelength 1950 nm to both sides, providing a broader spectrum width of SCG. Further studies revealed that the supercontinuum generated by pumping a CS_2 single-hole liquid core optical fiber (LCOF) with a 1.95 μm laser is robust over a large temperature range (15 °C–45 °C). Furthermore, the optimal temperature to obtain the broadest SC is 15 °C, and such

optimal temperature is independent on the pump power. The effect of pump power on SCG was also investigated. The result tells that at low pump power (such as $P_0 = 4$ kW) the coherence of the generated is independent on the temperature, while at high pump power (such as $P_0 = 40$ kW) the coherence of the long-wave (around 2600 nm) tends to be deteriorated at low temperature (e.g., 10 °C). The simulation method and the study results could provide a guide for optimizing SCG by using LOCF, and also for a similar application.

It should be noted that, there are some issues which should be considered for practical application but not included in the simulation here. 1. The direct coupling efficiency from the single mode fiber (pump laser) to liquid core optical fiber (LCOF) is low (<25%) considering the mismatch on the numerical aperture. Therefore, a customized coupling unit should be designed and utilized to improve the coupling efficiency between SMF and LCOF in practical application. 2. To utilize the temperature-tuning effect on SCG, the LCOF should be placed on a closed chamber, which has heating and air-cooling blocks, as well as temperature sensing and feedback controlling unit.

References

[1] N. Granzow *et al.*, "Mid-infrared supercontinuum generation in As_2S_3-silica "nano-spike" step-index waveguide," *Opt. Exp.*, vol. 21, no. 9, pp. 10969–10977, Apr. 2013. [Online]. Available: http://www.opticsexpress.org/abstract.cfm?URI=oe-21-9-10969

[2] R. A. Robert, *The Supercontinuum Laser Source*, 3rd ed. New York, NY, USA: Springer, 2016.

[3] H. Kano and H. O. Hamaguchi, "Characterization of a supercontinuum generated from a photonic crystal fiber and its application to coherent Raman spectroscopy," *Opt. Lett.*, vol. 28, no. 23, pp. 2360–2362, May 2003.

[4] K. Imura, T. Nagahara, and H. Okamoto, "Near-field two-photon-induced photoluminescence from single gold nanorods and imaging of plasmon modes," *J. Phys. Chem. B*, vol. 109, no. 27, pp. 13214–13220, Mar. 2005. [Online]. Available: https://doi.org/10.1021/jp051631o

[5] M. E. Brezinski *et al.*, "Assessing atherosclerotic plaque morphology: Comparison of optical coherence tomography and high frequency intravascular ultrasound," *Heart*, vol. 77, no. 5, pp. 397–403, May 1997. [Online]. Available: http://heart.bmj.com/content/heartjnl/77/5/397

[6] L. V. Wang and S. Hu, "Photoacoustic tomography: In vivo imaging from organelles to organs," *Science*, vol. 335, no. 6075, pp. 1458–1462, Mar. 2012. [Online]. Available: http://science.sciencemag.org/content/sci/335/6075/1458

[7] G. Li, "Recent advances in coherent optical communication," *Adv. Opt. Photon.*, vol. 1, no. 2, pp. 279–307, Apr. 2009. [Online]. Available: http://josab.osa.org/abstract.cfm?URI=josab-19-4-753

[8] R. Salem *et al.*, "Mid-infrared supercontinuum generation spanning 1.8 octaves using step-index indium fluoride fiber pumped by a femtosecond fiber laser near 2 μm," *Opt. Exp.*, vol. 23, no. 24, pp. 30592–30602, Nov. 2015. [Online]. Available: http://www.opticsexpress.org/abstract.cfm?URI=oe-23-24-30592

[9] A. R. Johnson *et al.*, "Octave-spanning coherent supercontinuum generation in a silicon nitride waveguide," *Opt. Lett.*, vol. 40, no. 21, pp. 5117–5120, Nov. 2015. [Online]. Available: https://www.ncbi.nlm.nih.gov/pubmed/26512533

[10] A. V. Husakou and J. Herrmann, "Supercontinuum generation of higher-order solitons by fission in photonic crystal fibers," *Phys. Rev. Lett.*, vol. 87, no. 20, pp. 203901-1–203901-4, Nov. 2001.

[11] G. Genty, M. Lehtonen, and H. Ludvigsen, "Effect of cross-phase modulation on supercontinuum generated in microstructured fibers with sub-30 fs pulses," *Opt. Exp.*, vol. 12, no. 19, pp. 4614–4624, Sep. 2004. [Online]. Available: http://www.opticsexpress.org/abstract.cfm?URI=oe-12-19-4614

[12] T. Schreiber, T. V. Andersen, D. Schimpf, J. Limpert, and A. Tünnermann, "Supercontinuum generation by femtosecond single and dual wavelength pumping in photonic crystal fibers with two zero dispersion wavelengths," *Opt. Exp.*, vol. 13, no. 23, pp. 9556–9569, Nov. 2005. [Online]. Available: http://www.opticsexpress.org/abstract.cfm?URI=oe-13-23-9556

[13] S. Coen *et al.*, "Supercontinuum generation by stimulated Raman scattering and parametric four-wave mixing in photonic crystal fibers," *J. Opt. Soc. Amer. B*, vol. 19, no. 4, pp. 753–764, Apr. 2002. [Online]. Available: http://josab.osa.org/abstract.cfm?URI=josab-19-4-753

[14] A. V. Yulin, D. V. Skryabin, and P. S. J. Russell, "Four-wave mixing of linear waves and solitons in fibers with higher-order dispersion," *Opt. Lett.*, vol. 29, no. 20, pp. 2411–2413, Apr. 2004. [Online]. Available: http://ol.osa.org/abstract.cfm?URI=ol-29-20-2411

[15] H. Hu, W. Li, S. Ma, and N. K. Dutta, "Coherence properties of supercontinuum generated in dispersion-tailored lead-silicate microstructured fiber taper," *Fiber Integr. Opt.*, vol. 32, no. 3, pp. 209–221, May 2013. [Online]. Available: https://doi.org/10.1080/01468030.2013.765058

[16] A. Hasegawa and F. Tappert, "Transmission of stationary nonlinear optical pulses in dispersive dielectric fibers. I. Anomalous dispersion," *Appl. Phys. Lett.*, vol. 23, no. 3, pp. 142–143, Aug. 2003.

[17] Y. Kodama and A. Hasegawa, "Nonlinear pulse propagation in a monomode dielectric guide," *IEEE J. Quantum Electron.*, vol. QE-23, no. 5, pp. 510–524, May 1987.

[18] N. Akhmediev and M. Karlsson, "Cherenkov radiation emitted by solitons in optical fibers," *Phys. Rev. A*, vol. 51, no. 3, pp. 2602–2607, Mar. 1995.

[19] D. V. Skryabin and A. V. Gorbach, "Looking at a soliton through the prism of optical supercontinuum," *Rev. Mod. Phys.*, vol. 82, no. 82, pp. 1287–1299, Apr. 2010.

[20] A. Demircan and U. Bandelow, "Supercontinuum generation by the modulation instability," *Opt. Commun.*, vol. 244, nos. 1–6, pp. 181–185, Sep. 2005.

[21] A. Hasegawa, "Generation of a train of soliton pulses by induced modulational instability in optical fibers," *Opt. Lett.*, vol. 9, no. 7, pp. 288–290, Jul. 1984.
[22] A. Hasegawa and W. F. Brinkman, "Tunable coherent IR and FIR sources utilizing modulational instability," *IEEE J. Quantum Electron.*, vol. QE-16, no. 7, pp. 694–697, Jul. 1980.
[23] P. T. Dinda and K. Porsezian, "Impact of fourth-order dispersion in the modulational instability spectra of wave propagation in glass fibers with saturable nonlinearity," *J. Opt. Soc. Amer. B*, vol. 27, no. 6, pp. 1143–1152, Jun. 2010. [Online]. Available: http://josab.osa.org/abstract.cfm?URI=josab-27-6-1143
[24] J. M. Hickmann, S. B. Cavalcanti, N. M. Borges, E. A. Gouveia, and A. S. Gouveia-Neto, "Modulational instability in semiconductor-doped glass fibers with saturable nonlinearity," *Opt. Lett.*, vol. 18, no. 3, pp. 182–184, Feb. 1993. [Online]. Available: http://ol.osa.org/abstract.cfm?URI=ol-18-3-182
[25] R. V. J. Raja, K. Porsezian, and K. Nithyanandan, "Modulational-instability-induced supercontinuum generation with saturable nonlinear response," *Phys. Rev. A*, vol. 82, no. 1, pp. 013825-1–013825-6, Jul. 2010. [Online]. Available: https://link.aps.org/doi/10.1103/PhysRevA.82.013825
[26] A. V. Husakou and J. Herrmann, "Supercontinuum generation, four-wave mixing, and fission of higher-order solitons in photonic-crystal fibers," *J. Opt. Soc. Amer. B*, vol. 19, no. 9, pp. 2171–2182, Sep. 2002. [Online]. Available: http://josab.osa.org/abstract.cfm?URI=josab-19-9-2171
[27] R. Vasantha Jayakantha Raja, A. Husakou, J. Hermann, and K. Porsezian, "Supercontinuum generation in liquid-filled photonic crystal fiber with slow nonlinear response," *J. Opt. Soc. Amer. B*, vol. 27, no. 9, pp. 1763–1768, Sep. 2010. [Online]. Available: http://josab.osa.org/abstract.cfm?URI=josab-27-9-1763
[28] P. Domachuk *et al.*, "Over 4000 nm bandwidth of mid-IR supercontinuum generation in sub-centimeter segments of highly nonlinear tellurite PCFs," *Opt. Exp.*, vol. 16, no. 10, pp. 7161–7168, May 2008. [Online]. Available: http://www.opticsexpress.org/abstract.cfm?URI=oe-16-10-7161
[29] C. Conti, M. A. Schmidt, P. S. Russell, and F. Biancalana, "Highly noninstantaneous solitons in liquid-core photonic crystal fibers," *Phys. Rev. Lett.*, vol. 105, no. 26, pp. 263902-1–263902-4, Dec. 2010. [Online]. Available: https://link.aps.org/doi/10.1103/PhysRevLett.105.263902
[30] M. Chemnitz *et al.*, "Hybrid soliton dynamics in liquid-core fibres," *Nat. Commun.*, vol. 8, no. 1, pp. 1–11, May 2017. [Online]. Available: https://doi.org/10.1038/s41467-017-00033-5
[31] H. El-Kashef, "Optical and electrical properties of materials," *Rev. Sci. Instrum.*, vol. 65, no. 6, pp. 2056–2061, Feb. 1994. [Online]. Available: https://www.ncbi.nlm.nih.gov/pubmed/24663448
[32] G. J. Raj, R. V. J. Raja, N. Nagarajan, and G. Ramanathan, "Tunable broadband spectrum under the influence of temperature in IR region using CS_2 core photonic crystal fiber," *J. Lightw. Technol.*, vol. 34, no. 15, pp. 3503–3509, Aug. 2016. [Online]. Available: http://jlt.osa.org/abstract.cfm?URI=jlt-34-15-3503
[33] M. Koshiba and K. Saitoh, "Structural dependence of effective area and mode field diameter for holey fibers," *Opt. Exp.*, vol. 11, no. 15, pp. 1746–1756, Jul. 2003.
[34] M. Koshiba and Y. Tsuji, "Curvilinear hybrid edge/nodal elements with triangular shape for guided-wave problems," *J. Lightw. Technol.*, vol. 8, no. 5, pp. 737–743, May 2000.
[35] A. Cucinotta, S. Selleri, L. Vincetti, and M. Zoboli, "Perturbation analysis of dispersion properties in photonic crystal fibers through the finite element method," *J. Lightw. Technol.*, vol. 20, no. 8, pp. 1433–1442, Jan. 2002. [Online]. Available: http://jlt.osa.org/abstract.cfm?URI=jlt-20-8-1433
[36] K. Saitoh, N. Florous, and M. Koshiba, "Ultra-flattened chromatic dispersion controllability using a defected-core photonic crystal fiber with low confinement losses," *Opt. Exp.*, vol. 13, no. 21, pp. 8365–8371, Oct. 2005. [Online]. Available: http://www.opticsexpress.org/abstract.cfm?URI=oe-13-21-8365
[37] G. P. Agrawal, *Nonlinear Fiber Optics*, 4th ed. San Diego, CA, USA: Academic, 2010.
[38] X. Gai, D.-Y. Choi, S. Madden, Z. Yang, R. Wang, and B. Luther-Davies, "Supercontinuum generation in the mid-infrared from a dispersion-engineered As_2S_3 glass rib waveguide," *Opt. Lett.*, vol. 37, no. 18, pp. 3870–3872, Sep. 2012. [Online]. Available: http://ol.osa.org/abstract.cfm?URI=ol-37-18-3870
[39] T. A. Birks, J. C. Knight, and P. S. J. Russell, "Endlessly single-mode photonic crystal fiber," *Opt. Lett.*, vol. 22, no. 13, pp. 961–963, Jul. 1997.
[40] F. Poletti and P. Horak, "Dynamics of femtosecond supercontinuum generation in multimode fibers," *Opt. Exp.*, vol. 17, no. 8, pp. 6134–6147, Apr. 2009.
[41] A. B. Salem, A. Trichili, R. Cherif, and M. Zghal, "Rigorous study of supercontinuum generation in few mode fibers," *Appl. Opt.*, vol. 55, no. 16, pp. 4317–4322, Jun. 2016. [Online]. Available: http://ao.osa.org/abstract.cfm?URI=ao-55-16-4317
[42] R. Zhang, J. Teipel, and H. Giessen, "Theoretical design of a liquid-core photonic crystal fiber for supercontinuum generation," *Opt. Exp.*, vol. 14, no. 15, pp. 6800–6812, Jul. 2006. [Online]. Available: http://www.opticsexpress.org/abstract.cfm?URI=oe-14-15-6800
[43] J. Hult, "A fourth-order Runge–Kutta in the interaction picture method for simulating supercontinuum generation in optical fibers," *J. Lightw. Technol.*, vol. 25, no. 12, pp. 3770–3775, Dec. 2007.
[44] J. M. Dudley and S. Coen, "Coherence properties of supercontinuum spectra generated in photonic crystal and tapered optical fibers," *Opt. Lett.*, vol. 27, no. 13, pp. 1180–1182, Jul. 2002.
[45] J. M. Dudley, G. Genty, and S. Coen, "Supercontinuum generation in photonic crystal fiber," *Rev. Mod. Phys.*, vol. 78, no. 4, pp. 1135–1184, Oct. 2006. [Online]. Available: https://link.aps.org/doi/10.1103/RevModPhys.78.1135
[46] I. A. Heisler, R. R. B. Correia, T. Buckup, S. L. Cunha, and N. P. da Silveira, "Time-resolved optical Kerr-effect investigation on CS2/polystyrene mixtures," *J. Chem. Phys.*, vol. 123, no. 5, pp. 054509-1–054509-6, Jun. 2005. [Online]. Available: https://aip.scitation.org/doi/abs/10.1063/1.1994850